Available online at www.sciencedirect.com
SCIENCE DIRECT®
Mathematics and Computers in Simulation 65 (2004) 385–397
MATHEMATICS AND COMPUTERS IN SIMULATION
www.elsevier.com/locate/matcom

Quantum confinement phenomena in nanowire superlattice structures

M. Willatzen [a,*], R.V.N. Melnik [a], C. Galeriu [b], L.C. Lew Yan Voon [b]

[a] *Mads Clausen Institute for Product Innovation, University of Southern Denmark, Grundtvigs Alle 150, DK-6400 Sønderborg, Denmark*

[b] *Department of Physics, Worcester Polytechnic Institute, 100 Institute Road, Worcester, MA 01609, USA*

Abstract

Nanowire superlattices (NWSLs) are objects with a wide range of potential applications in nanoscale electronics and photonics. These objects are already grown experimentally in laboratories and studies of their properties represent an important task in nanotechnology research. Tools of mathematical modelling provide a powerful means for studying these fascinating structures with an ultimate goal of predicting their properties and understanding their limits. In this paper, we analyse finite nanowire GaAs/$Al_{0.3}Ga_{0.7}As$ superlattice structures with a cylindrical cross-section and determine their electronic eigenstates and energy eigenvalues. We analyse in detail the qualitative differences, in terms of wavefunctions and energy eigenvalues, between structures containing the same number of barriers and wells (asymmetrical) and structures where the number of barrier layers is one above the number of well layers (symmetrical). We demonstrate that asymmetrical NWSL structures have well-pronounced qualitative and quantitative differences as compared to both symmetrical NWSL structures and infinite periodic NWSL structures. We show also that there exists a critical radius R_c for quantum confinement, that is the NWSL ground state is confined in GaAs ($Al_{0.3}Ga_{0.7}As$) for a nanowire of radius R above (below) R_c. In the specific case where $R = R_c$, the ground state is smeared out over the entire NWSL structure.

Keywords: Nanowire superlattices; Nanotechnology; Barrier layers

1. Introduction

Semiconductor technology today allows finite-length modulated quantum-wire heterostructures to be grown in what is known as nanowire superlattice (NWSL) structures. These structures can be grown using various growth techniques most of which are based upon a nanocluster catalyst. Experimentalists have considered GaAs/GaP [6], Si/SiGe [12], InAs [2] and ZnSe/CdSe [9] structures (in the latter case, using atomic layer deposition). They have demonstrated that longitudinally modulated nanowires can

* Corresponding author. Tel.: +45-6550-1682; fax: +45-6550-1660.
E-mail address: willatzen@mci.sdu.dk (M. Willatzen).

0378-4754/$30.00 © 2004 IMACS. Published by Elsevier B.V. All rights reserved.
doi:10.1016/j.matcom.2004.01.010

be grown [2,6,12] with nanowire radii of 200–400 Å and layer width of 150–1000 Å. NWSL structures are expected to find applications as nanobar codes, waveguides, lasers and light-emitting diodes. In particular, it has been argued that NWSL structures may show better characteristic properties as compared to plain nanowires [11] due to the coupling of superlattice longitudinal confinement to the nanowire radial confinement. These characteristic properties include the extremely polarised photoluminescence of a NWSL and the non-Ohmic conductance of a NWSL with a single barrier.

In the present work, the finite nanowire superlattice problem was examined using a one-band model for electrons in the conduction band. Thus, the approach taken here is expected to give accurate results for the GaAs/$Al_{0.3}Ga_{0.7}As$ nanostructures where non-parabolicity effects are of minor importance due to the large bandgap present.

We discuss the wavefunction properties of the various NWSL structures and show that the eigenvalues found for a finite symmetrical structure converges towards the Kronig–Penney (KP) model results for eigenvalues if the number of wells increases towards infinity. Moreover, we also found that the energy spectrum for finite NWSL symmetrical structures with the number of unit cells above 6–7 is similar to the energy spectrum found in the Kronig–Penney model case. There are qualitative and quantitative differences when considering asymmetrical NWSL structures with a barrier layer at one end and a well layer at the other end as compared to symmetrical finite NWSL structures and the infinite periodic (Kronig–Penney) NWSL structure. It is verified that a critical radius of the NWSL structure exists, i.e., for NWSL radii above (below) the critical radius the effective potential for longitudinal confinement is higher (lower) in $Al_{0.3}Ga_{0.7}As$ as compared to GaAs. As a consequence, ground-state envelope functions are predominantly located in the GaAs ($Al_{0.3}Ga_{0.7}As$) material layers for $R > R_c$ ($R < R_c$).

2. Theory

The nanowire superlattice was modelled as an ideal cylinder with sharp modulations in the longitudinal (or z-direction) (Fig. 1). The electronic structure can, in general, be found based on a multiband $\vec{k} \cdot \vec{p}$ model for the envelope function [1,3]:

$$\underline{H}\underline{\psi} = E\underline{\psi}, \tag{1}$$

where $\underline{H}$ is a $n \times n$ Hamiltonian matrix containing corresponding Schrödinger's partial differential operators, $\underline{\psi}$ the associated envelope-function vector (dimension $n \times 1$) and E the energy eigenvalue.

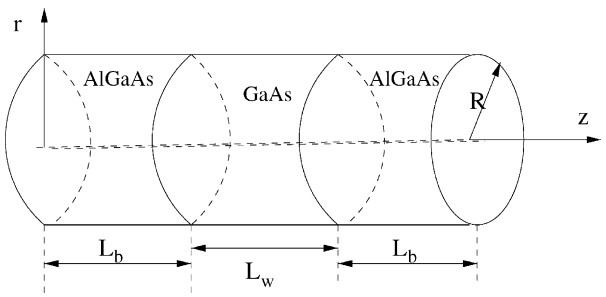

Fig. 1. Schematic representation of nanowire geometry.

The value n is the number of bands included in the multiband analysis usually 2 (S-type conduction band), 4 (P-type heavy-hole and light-hole valence bands), 6 (P-type heavy-hole, light-hole and split-off valence bands), or 8 (S-type conduction band and P-type heavy-hole, light-hole and split-off valence bands) accounting for the two electron and hole spin orientations.

It is, however, a good approximation to employ a one-band $\vec{k}\cdot\vec{p}$ model (equivalent to the above-mentioned case with two S-type conduction bands due to spin degeneracy) so as to calculate the conduction bandstructure of GaAs/$Al_{0.3}Ga_{0.7}$As heterostructure systems for the following reasons: (a) the GaAs/$Al_{0.3}Ga_{0.7}$As nanowire superlattice system is characterised by a direct bandgap allowing $\vec{k}\cdot\vec{p}$ theory to be applied directly; (b) the large bandgap of GaAs/$Al_{0.3}Ga_{0.7}$As systems ensures that band-mixing effects are of minor importance when calculating the conduction band states; and (c) strain effects are absent in GaAs/$Al_{0.3}Ga_{0.7}$As heterostructures. With these comments in mind, it is appropriate to determine the electronic structure by solving the one-dimensional Ben Daniel–Duke equation [1]:

$$-\frac{\hbar^2}{2}\nabla\cdot\left[\frac{1}{m(\boldsymbol{r})}\nabla\psi(\boldsymbol{r})\right]+V(\boldsymbol{r})\psi(\boldsymbol{r})=E\psi(\boldsymbol{r}), \tag{2}$$

where $V(\boldsymbol{r})$ is the potential experienced by the electron (will be taken to be infinite outside the wire (vacuum) and piecewise constant inside), $m(\boldsymbol{r})$ the effective mass in each superlattice layer, ψ the wavefunction and E the energy. Eq. (2) is supplemented by Dirichlet boundary conditions (on the surface of the nanowire structures) which correspond to the case where the nanostructure environment is vacuum. The above model is valid for the conduction band of large-gap cubic semiconductors [1], and our results are reported here for the latter case.

2.1. Formulation of separable differential equations

It is possible to separate the differential equation in Eq. (2) in ordinary differential equations as will be explained next. Let us write:

$$\psi(\vec{r})=\Phi(\phi)\,J(r)\,Z(z). \tag{3}$$

Insertion of Eq. (3) in Eq. (2) and restructuring leads to:

$$\begin{aligned}-\frac{\hbar^2}{2}\frac{\mathrm{d}}{\mathrm{d}z}\left(\frac{1}{m_\mathrm{e}(z)}\frac{\mathrm{d}Z}{\mathrm{d}z}\right)\frac{m_\mathrm{e}(z)}{Z(z)}+(V_\mathrm{e}(z)-E)m_\mathrm{e}(z)&=-\frac{\hbar^2}{2}\frac{1}{r}\frac{\mathrm{d}}{\mathrm{d}r}\left(r\frac{\mathrm{d}J}{\mathrm{d}r}\right)\frac{1}{J(r)}+\frac{\hbar^2}{2r^2}\frac{1}{\Phi(\phi)}\frac{\mathrm{d}^2\Phi}{\mathrm{d}\phi^2}\\&\equiv-\frac{\hbar^2q^2}{2},\end{aligned} \tag{4}$$

where q is a separation constant. The second equality in Eq. (4) allows further separation of the problem:

$$\frac{\hbar^2}{2}\frac{1}{r}\frac{\mathrm{d}}{\mathrm{d}r}\left(r\frac{\mathrm{d}J}{\mathrm{d}r}\right)\frac{r^2}{J(r)}+\frac{\hbar^2q^2r^2}{2}=-\frac{\hbar^2}{2}\frac{1}{\Phi(\phi)}\frac{\mathrm{d}^2\Phi}{\mathrm{d}\phi^2}\equiv\frac{\hbar^2}{2}l^2, \tag{5}$$

where l is a second separation constant.

Eqs. (4) and (5) can be restated as three ordinary differential equations:

$$\frac{\mathrm{d}^2\Phi(\phi)}{\mathrm{d}\phi^2} + l^2\Phi(\phi) = 0, \qquad r = \frac{\mathrm{d}}{\mathrm{d}r}\left(r\frac{\mathrm{d}J}{\mathrm{d}r}\right) + [q^2r^2 - l^2]J(r) = 0,$$
$$\frac{\mathrm{d}}{\mathrm{d}z}\left(\frac{1}{m(z)}\frac{\mathrm{d}Z(z)}{\mathrm{d}z}\right) + \frac{2}{\hbar^2}\left[E - V(z) - \frac{\hbar^2q^2}{2m(z)}\right]Z(z) = 0. \tag{6}$$

The solution to the first of Eq. (6)—the angular equation—is trivial, $\Phi(\phi) = \mathrm{e}^{\pm \mathrm{i}l\phi}$, with l an integer. The solution to the second of Eq. (6)—the radial equation—is a Bessel function of the first kind, with the wave number q determined by the boundary condition $J_l(qR) = 0$, where R is the radius of the NWSL. A second solution to the radial equation is the Neumann function $N_l(qr)$ but the latter solution can be discarded because it diverges at $r = 0$. The third equation of Eq. (6) is the longitudinal equation.

Note, as a more general case, that when the potential V and/or the effective mass m is a function of both z and r, the general three-dimensional problem (Eq. (2)) can be separated in the azimuthal co-ordinate ϕ only, and we obtain:

$$-\frac{\hbar^2}{2}\frac{\partial}{\partial z}\left(\frac{1}{m(z,r)}\frac{\partial\chi_l}{\partial z}\right) - \frac{\hbar^2}{2}\frac{1}{r}\frac{\partial}{\partial r}\left(\frac{r}{m(z,r)}\frac{\partial\chi_l}{\partial r}\right) + \frac{\hbar^2}{2m(z,r)}\frac{l^2}{r^2}\chi_l(z,r) + V(z,r)\,\chi_l(z,r)$$
$$= E\,\chi_l(z,r), \tag{7}$$

with $\psi(r,\phi,z) = \chi_l(z,r)\exp(\mathrm{i}l\phi)$. This particular case is of physical relevance when, e.g., the NWSL structure is embedded in a material different from vacuum such that simple Dirichlet boundary conditions do not apply any longer. Note that all results presented in Section 4 have been obtained with a more general mathematical problem (Eq. (7)).

2.2. Kronig–Penney model for a nanowire superlattice structure

A simple quasi-analytical solution to the longitudinal equation can be provided in the case where the nanowire superlattice structure extends infinitely along the $+z$-direction and the $-z$-direction. In this case, Bloch's theorem can be applied in the z-direction due to the periodicity of the NWSL structure. The NWSL unit cell consists of a single layer GaAs and a neighbouring (single) layer of $Al_{0.3}Ga_{0.7}As$.

In Fig. 2, a plot of the infinite heterostructure potential $V(z)$ is shown as a function of position. The boundary conditions fulfilled by the envelope function are:

$$\psi_{\mathrm{II}}(0) = \psi_{\mathrm{I}}(0), \qquad \frac{1}{m_{\mathrm{II}}}\psi'_{\mathrm{II}}(0) = \frac{1}{m_{\mathrm{I}}}\psi'_{\mathrm{I}}(0), \tag{8}$$

where the second equation follows from the structure of the first term in the longitudinal equation (Eq. (6)).

Evidently, the general solution to the longitudinal equation in regions I and II becomes:

$$\psi_{\mathrm{I}}(z) = A\,\mathrm{e}^{k_{\mathrm{I}}z} + B\,\mathrm{e}^{-k_{\mathrm{I}}z}, \qquad \psi_{\mathrm{II}}(z) = C\,\mathrm{e}^{\mathrm{i}k_{\mathrm{II}}z} + D\,\mathrm{e}^{-\mathrm{i}k_{\mathrm{II}}z}, \tag{9}$$

where A, B, C and D are constants, and

$$k_{\mathrm{II}}^2 = \frac{2m_{\mathrm{II}}}{\hbar^2}E, \qquad k_{\mathrm{I}}^2 = \frac{2m_{\mathrm{I}}}{\hbar^2}(V_0 - E). \tag{10}$$

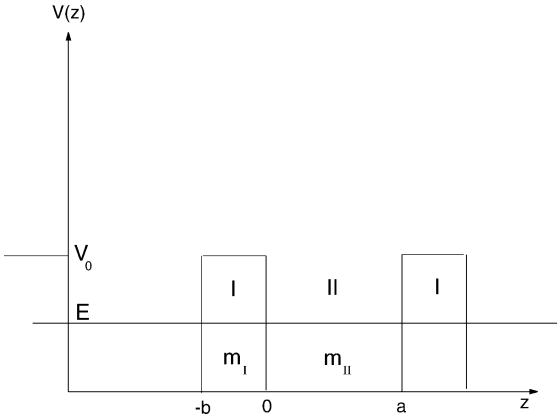

Fig. 2. Potential for the infinite nanowire superlattice structure.

Here, V_0 (or 0) is the conduction band-edge potential of $Al_{0.3}Ga_{0.7}As$ (or GaAs). Next, employing Bloch periodicity gives:

$$\psi_K(z+a+b) = \mathrm{e}^{\mathrm{i}K(a+b)}\,\psi_K(z), \tag{11}$$

where K is a Bloch constant. With reference to Fig. 2, Eq. (11) reads:

$$\psi_{K,\mathrm{II}}(a) = \mathrm{e}^{\mathrm{i}K(a+b)}\,\psi_{K,\mathrm{I}}(-b), \qquad \frac{1}{m_{\mathrm{II}}}\psi'_{K,\mathrm{II}}(a) = \frac{1}{m_I}\mathrm{e}^{\mathrm{i}K(a+b)}\,\psi'_{K,\mathrm{I}}(-b). \tag{12}$$

The above boundary conditions (Eqs. (7) and (12)) lead to the determinental equation:

$$\begin{vmatrix} 1 & 1 & -1 & -1 \\ \mathrm{i}k_{\mathrm{II}}/m_{II} & -\mathrm{i}k_{\mathrm{II}}/m_{\mathrm{II}} & -k_{\mathrm{I}}/m_{\mathrm{I}} & k_{\mathrm{I}}/m_{\mathrm{I}} \\ \mathrm{e}^{\mathrm{i}k_{\mathrm{II}}a} & \mathrm{e}^{-\mathrm{i}k_{\mathrm{II}}a} & -\mathrm{e}^{\mathrm{i}K(a+b)-k_{\mathrm{I}}b} & -\mathrm{e}^{\mathrm{i}K(a+b)+k_{\mathrm{I}}b} \\ \dfrac{\mathrm{i}k_{\mathrm{II}}\,\mathrm{e}^{\mathrm{i}k_{\mathrm{II}}a}}{m_{\mathrm{II}}} & \dfrac{-\mathrm{i}k_{\mathrm{II}}\,\mathrm{e}^{-\mathrm{i}k_{\mathrm{II}}a}}{m_{\mathrm{II}}} & \dfrac{-k_{\mathrm{I}}\,\mathrm{e}^{\mathrm{i}K(a+b)-k_{\mathrm{I}}b}}{m_{\mathrm{I}}} & \dfrac{k_{\mathrm{I}}\,\mathrm{e}^{\mathrm{i}K(a+b)+k_{\mathrm{I}}b}}{m_{\mathrm{I}}} \end{vmatrix} = 0, \tag{13}$$

where Eq. (10) has been used. A non-trivial solution is found whenever Eq. (13) is fulfilled, i.e.:

$$\cos K(a+b) = \cos(k_{\mathrm{II}}a)\cosh(k_{\mathrm{I}}b) + \frac{(k_{\mathrm{I}}^2/m_{\mathrm{I}}^2 - k_{\mathrm{II}}^2/m_{\mathrm{II}}^2)}{2(k_{\mathrm{II}}/m_{\mathrm{II}})(k_{\mathrm{I}}m_{\mathrm{I}})}\sin(k_{\mathrm{II}}a)\sinh(k_{\mathrm{I}}b). \tag{14}$$

2.3. Critical radius

In the following section, we shall describe some very interesting consequences of the form of the longitudinal equation (third of Eq. (6)). First, observe that the solution to the radial equation (second of Eq. (6)) depends upon only one of the geometrical parameters of the NWSL, the radius R. The possible discrete set of q values are determined by R and, of course, the value of l since $J_l(qR) = 0$. Once q is determined, the effective potential in the longitudinal equation:

$$V^{\mathrm{eff}} = V(z) + \frac{q^2}{m(z)}, \tag{15}$$

is fixed. For typical semiconductor heterostructures, the well mass m_{W} is smaller than the barrier mass m_{B} such that the effective potential barrier height V^{eff} decreases as the radius is decreased:

$$V_0^{\mathrm{eff}} = V_0 - \frac{j_{ln}^2}{R^2}\left(\frac{1}{m_{\mathrm{W}}} - \frac{1}{m_{\mathrm{B}}}\right), \tag{16}$$

and it can be zero or negative if:

$$R^2 \leq \frac{m_{\mathrm{B}} - m_{\mathrm{W}}}{m_{\mathrm{B}} m_{\mathrm{W}} V_0} j_{ln}^2 \equiv R_{\mathrm{c}}^2, \tag{17}$$

where j_{ln} is the nth zero of J_l. Hence, below a critical radius R_{c}, the barrier layer now acts as the well layer and vice versa; we call the latter an inverted structure. While various types of localisation have been studied in type II systems, the current one is different in origin and can occur in both type I and II systems [7].

3. Numerical technique for eigenvalue PDE problems of Ben Daniel–Duke type

Problem (7) is supplemented by appropriate boundary conditions. In our case, the appropriate choice is based on the assumption that the nanostructure external environment is vacuum which corresponds to Dirichlet boundary conditions on the surface of the nanowire. Due to the presence of alternating layers of barriers and wells in the structure, the formulated model should be understood in a weak sense. The only additional assumptions required are continuity of the wave function and the standard relationship for its gradient at the interface between two different layers of the structure [5,8]. These assumptions are formulated in a way analogous to that expressed by (8). The finite element discretisation was applied to project the variational form of the problem onto a finite-dimensional space, and all integrals were approximated with Gaussian quadratures. As a result, the problem was reduced to the following generalised eigenvalue problem:

$$Au = \lambda Bu, \tag{18}$$

where matrices $\boldsymbol{A}$ and $\boldsymbol{B}$ are $N \times N$ matrices, $\boldsymbol{u}$ the vector of unknowns of dimensionality N, and N the number of nodes in which the solution to the problem (7) is being sought. More precisely, after discretisation we arrive at an algebraic eigenvalue problem (18) with $\boldsymbol{A}$ resulted from a second order discrete approximation to $-\bar{h}^2/2\nabla \cdot [1/m(\boldsymbol{r})\nabla\psi(\boldsymbol{r})]$ and $\boldsymbol{B} = E - V$.

Computational domains of interest are symmetric with respect to the z-axis, where we imposed Neumann's boundary conditions if $l = 0$, and Dirichlet boundary conditions otherwise. The rest of the structures are bordered with vacuum, and hence, as we have already mentioned, Dirichlet boundary conditions were imposed in that case. In computations that we have performed the number of elements varied from around 5000 up to 200,000 and the number of nodes varied from several thousands to around 150,000, depending on the size of the structure and the required accuracy. The solution to Eq. (18) was found in an iterative manner by using the Krylov subspace projective methodology. We have used an orthogonal projection [10]; in particular, the core of the solver is the spectral Arnoldi iteration method. While the standard QR methodology may destroy the sparsity of the matrix $\boldsymbol{A}$ obtained as a result of discretisation, the spectral Arnoldi iteration method keeps this important property. At the kth iteration of the standard QR methodology we need to overwrite the vector $\boldsymbol{A}^{k-1}\vec{u}_n$ with $\boldsymbol{A}^{k}\vec{u}_n$. In the methodology

used here, we keep track of the entire set of the previous vectors, generating a Krylov subspace in the following form:

$$K_m\{\boldsymbol{A}, \vec{u}_n\} = \text{span}\{\vec{u}_n, \boldsymbol{A}\vec{u}_n, \ldots, \boldsymbol{A}^{m-1}\vec{u}_n\}. \tag{19}$$

We searched for all eigenvalues of the problem in the given interval. The boundary estimates for the interval follows directly from the physics of the problem, and in the case analysed here they are 0 eV for the lower bound (the GaAs conduction band edge) and 0.23 eV for the upper bound (the $Al_{0.3}Ga_{0.7}As$ potential barrier). The procedure was implemented in the Matlab-based Femlab environment [4]. Adaptive mesh refinements were used to ensure convergence on a sequence of grids. The results obtained from our calculations were compared with those available for the Kronig–Penney model describing infinite NWSLs, as we explained in Section 2.2.

4. Results and discussion

In the following section, we discuss only states with azimuthal symmetry, i.e., states for which $l = 0$. It must be emphasised, however, that states with $l \neq 0$ can be found in a completely analogous manner—without any problems—using the procedure described in Section 3. Our discussion that follows is based on the NWSL structures that consist of 50 Å GaAs well layers (L_w in Fig. 1) and 50 Å $Al_{0.3}Ga_{0.7}As$ barrier layers (L_b in Fig. 1) stacked in an alternate fashion. The radius, R, is 100 Å for all layers, i.e., 100 Å for the whole NWSL layer (Fig. 1). We employed the finite element method (FEM) so as to calculate electron eigenvalues and eigenstates for a series of finite NWSL structures with a cylindrical cross-section. The NWSL structures considered are symmetrical or asymmetrical (with respect to a centre plane of the nanostructure) in the following sense. For the symmetrical structures, we assumed $N + 1$ layers in the NWSL structure are barrier layers. Then, N layers are well layers where N is an integer (see Fig. 1). Similarly, for the asymmetrical structure, we assumed N layers in the NWSL structure are barrier layers, then N layers are well layers where N is an integer. The former structures are symmetrical because a mirror reflection around the centre plane of the structure leaves the structure unchanged while this is not the case for the latter (asymmetrical) structures.

4.1. Symmetry characteristics of NWSL structures

In Fig. 3, we show the two bound states found for the asymmetrical structure with two well layers. These states have energies 0.1046 and 0.1489 eV, respectively, and both states have zero nodes along the radial direction. Since the mirror reflection operator about the centre plane is not a symmetry for the asymmetrical structure, neither the ground state nor the first excited state will be symmetric (or antisymmetric) with respect to the same centre plane. This is clearly observed in Fig. 3. The reason behind the rather large energy difference between the two states is the following. The ground state is predominantly located in the GaAs well layer sandwiched between two $Al_{0.3}Ga_{0.7}As$ barrier layers (with potential barriers of 0.23 eV) while the excited state is predominantly located in the GaAs well layer sandwiched by a $Al_{0.3}Ga_{0.7}As$ barrier layer and vacuum (with potentials 0.23 eV and ∞, respectively).

In Fig. 4, we compare numerical results for the ground state and the first excited state of: (a) the symmetrical structure consisting of five well layers and six barrier layers; and (b) the asymmetrical structure consisting of five well layers and five barrier layers. It is evident that the ground state (first excited state)

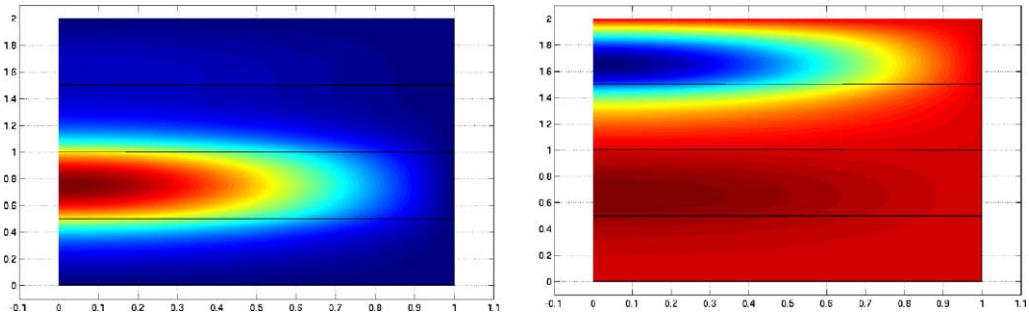

Fig. 3. Asymmetric nanowire with two wells: ground and first excited states.

of the former structure is symmetric (antisymmetric) with respect to a mirror reflection in the centre plane of the NWSL structure due to the fact that the mirror reflection operator is a symmetry for the symmetrical structure. As mentioned above, no such mirror reflection symmetry exists for the asymmetrical structure and therefore the ground state (first excited state) is also not symmetric (antisymmetric) with respect to a mirror reflection in the centre plane. It follows by inspection of the various eigenmodes and eigenvalues for the asymmetrical structure that three eigenstates have almost the same energy as the ground state—all of them between 0.10 and 0.11 eV above the conduction-band edge of GaAs (in the following energies are calculated with the GaAs conduction-band edge as a reference). This is a consequence of the fact that the symmetrical structure consists of five wells and that four of these wells are located between

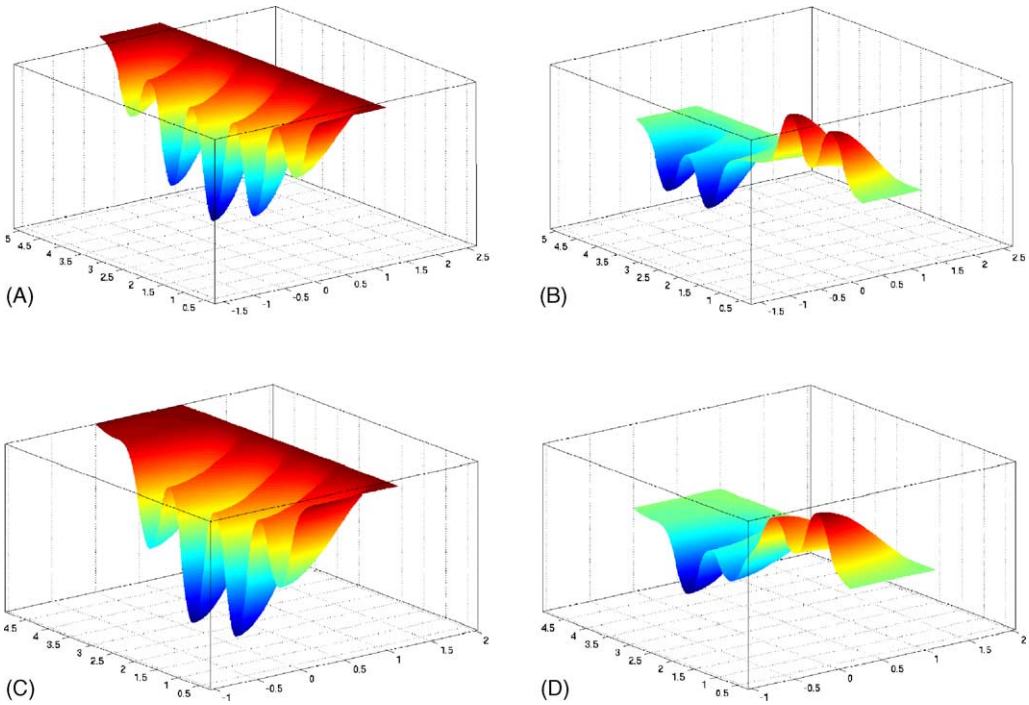

Fig. 4. Symmetric (top) and asymmetric nanowire (bottom) with five wells: ground and first excited states.

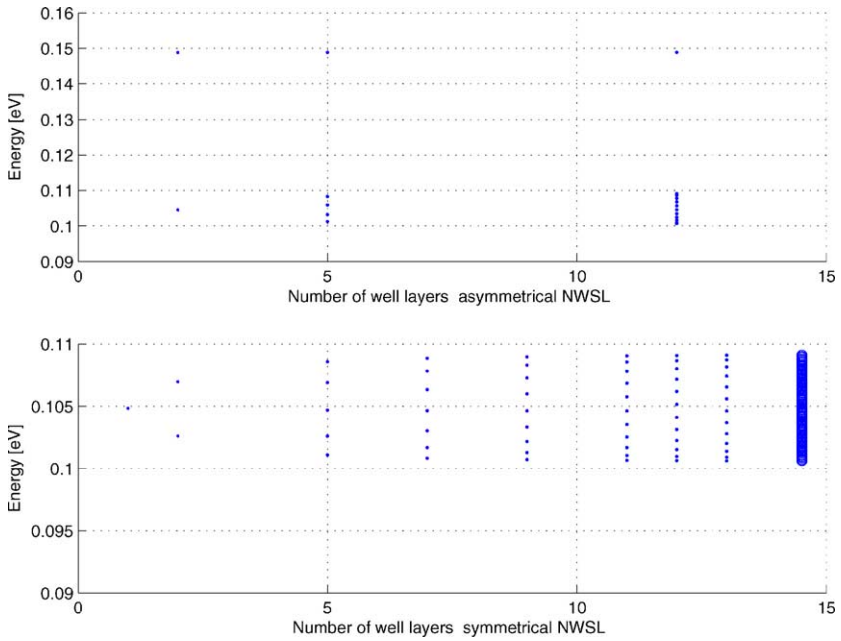

Fig. 5. Comparisons with the KP model. The KP model results are shown to the far right only for the symmetrical structure.

two barrier layers of $Al_{0.3}Ga_{0.7}As$. The first four states are all predominantly associated with these four wells. The remaining fifth state is, however, predominantly associated with the fifth well sandwiched between a $Al_{0.3}Ga_{0.7}As$ barrier layer and vacuum, and thus has a substantially higher energy (again refer to the discussion above). Returning to the symmetrical structure, note that here all five well layers are sandwiched between $Al_{0.3}Ga_{0.7}As$ layers, hence the five states associated with the well layers must have approximately the same energy (between 0.10 and 0.11 eV).

In Fig. 5, we plot energy eigenvalues as a function of the number of well layers for asymmetrical (top) and symmetrical (bottom) NWSL structures. The qualitative behaviour discussed above for symmetrical and asymmetrical structures can be seen in Fig. 5. Moreover, it is found that the energy eigenvalue range for the symmetrical structure approaches that of the Kronig–Penney model case (corresponding to an infinite number of unit cells where each unit cell consists of a single well layer and a single barrier layer) as $N \to \infty$. It is interesting to note that the state predominantly associated with the well layer sandwiched between vacuum and a $Al_{0.3}Ga_{0.7}As$ barrier layer—found in the asymmetrical structures only—finds no analogue in any symmetrical NWSL structure or in the KP structure due to different symmetry properties.

4.2. Critical radius and quantum confinement phenomena

We next discuss some implications of localisation for NWSL radii above, at and below the critical radius. In the present case with $m_W = 0.067m_0$ (GaAs), $m_B = 0.092m_0$ ($Al_{0.3}Ga_{0.7}As$). Hence, according to Eq. (17), the smallest critical radius (R_c calculated for $l = 0$ and $n = 1$) becomes 19.632 Å. It should be noted that although this is close to borderline for the applicability of $\vec{k} \cdot \vec{p}$ theory, it is well known that the

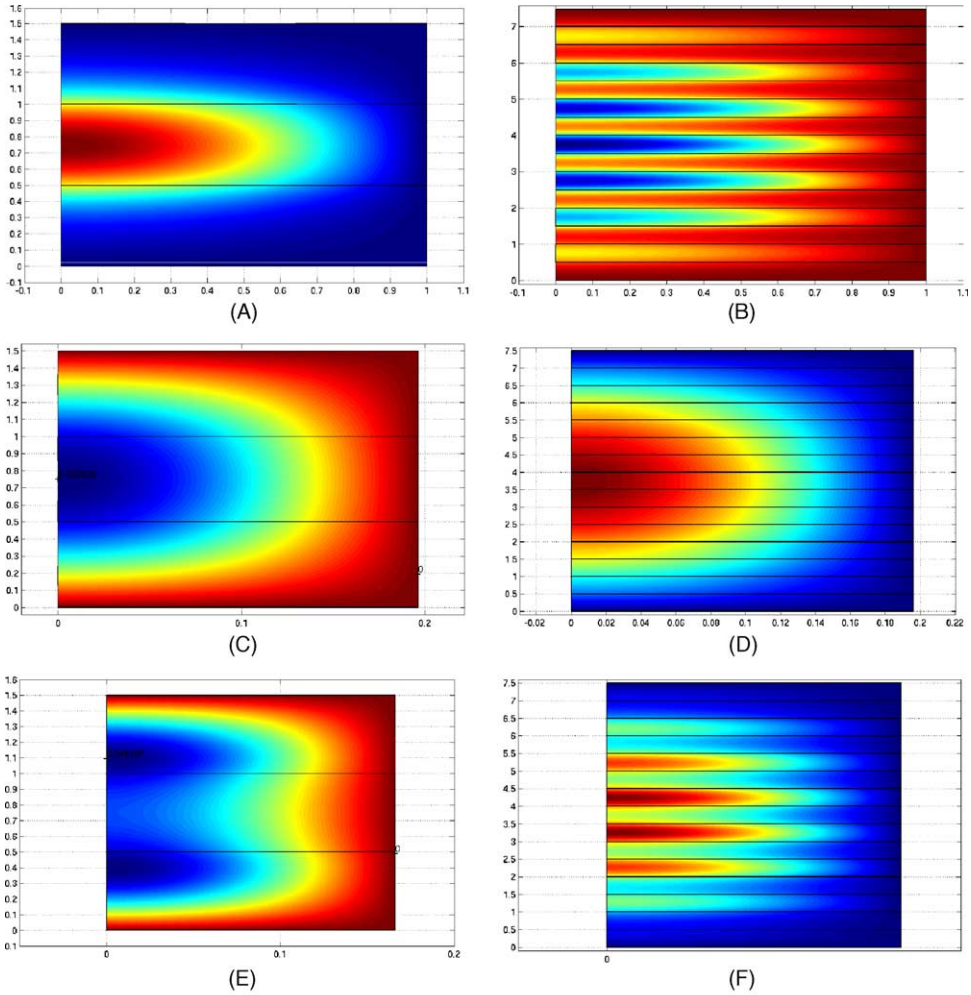

Fig. 6. Conduction-band ground state in GaAs/$Al_{0.3}Ga_{0.7}As$ symmetric NWSL structures. The left (right) plots are for NWSL structures with one (seven) GaAs material layers. The upper, middle and lower two plots are for NWSL structures with $R = 100$ Å $> R_c$, $R = R_c = 19.632$ Å and $R = 16.632$ Å $< R_c$, respectively.

small size does not invalidate this approximation qualitatively, but rather might introduce a slight chance in the quantitative results [3].

In Fig. 6, contour plots of the ground-state envelope functions for two symmetrical structures are shown with one and seven GaAs material layers for three values of the NWSL radius: $R > R_c$ (top), $R = R_c$ (middle), and $R < R_c$ (bottom). Consider first the case with $R = 100$ Å $> R_c$. It is evident that the ground state is predominantly located in the GaAs layers in both cases with one and seven GaAs material layers. This is expected since the effective potential is higher in the $Al_{0.3}Ga_{0.7}As$ layers as compared to the GaAs layers and the former (latter) region acts as barrier (well) material. Consider next the case with $R = R_c$. Here, the envelope function is smeared out over the central region of the NWSL structure

Table 1
Ground-state energies for GaAs/$Al_{0.3}Ga_{0.7}As$ NWSL structures with $R = 16.632\,Å < R_c$

GaAs material layers	Symmetrical NWSL (eV)	Asymmetrical NWSL (eV)
2	1.1502	1.1859
5	1.1442	1.1405
12	1.1403	1.1403

and decays towards the left and right ends of the NWSL structure (as a consequence of vacuum being next to the NWSL end regions). No material localisation occurs in the NWSL structure with seven GaAs layers (middle-right) as expected with an effective barrier potential V_0^{eff} equal to zero. In the lower two plots of Fig. 6, computed ground-state results for an inverted NWSL structure is shown corresponding to $R = 16.632\,Å < R_c$. Indeed, the envelope function is now predominantly located in the $Al_{0.3}Ga_{0.7}As$ region for the one and seven GaAs layer cases, i.e., the opposite localisation take place as compared to the localisation observed in the top plots of Fig. 6 where $R > R_c$. Notice also that the envelope function in the lower-left plot (with one GaAs material layer) is located predominantly in the $Al_{0.3}Ga_{0.7}As$ material layers but shifted towards (away from) the interface with the neighbouring GaAs layer (vacuum).

In Table 1, ground-state energies are given for the symmetrical NWSL structure with 2, 5 and 12 GaAs material layers in the case where $R = 16.632\,Å < R_c$ (inverted structure). Observe that the energies

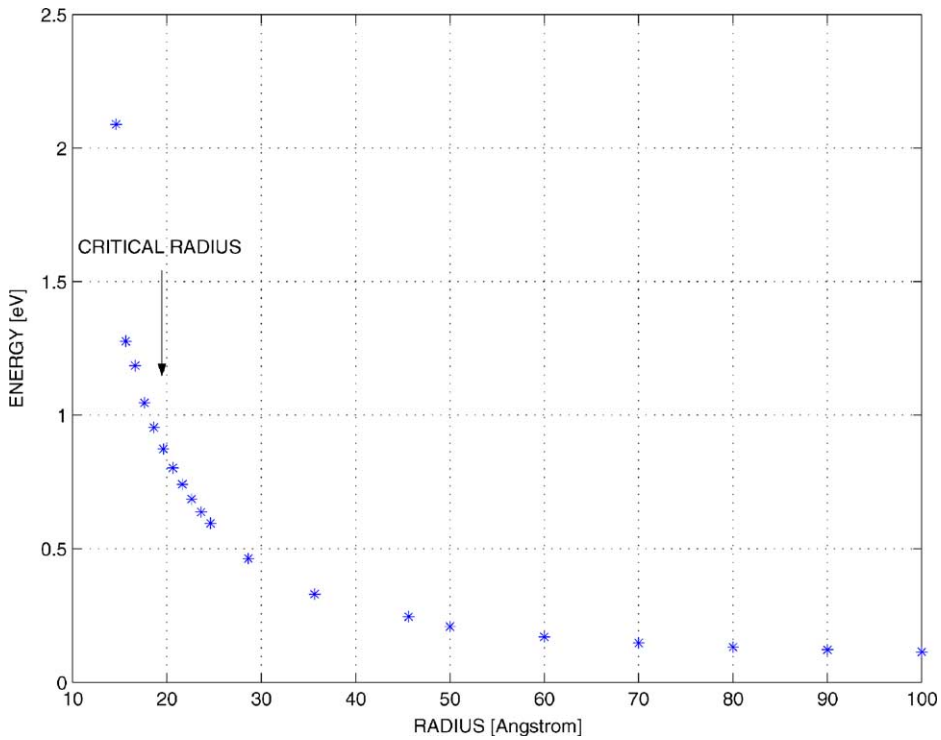

Fig. 7. Ground-state energy vs. NWSL radius for a GaAs/$Al_{0.3}Ga_{0.7}As$ asymmetrical NWSL structure with two GaAs material layers.

are high above (> 1 eV) the conduction band-edge of $Al_{0.3}Ga_{0.7}As$ being 0.24 eV due to the very small radius. In actual fact, the longitudinal equation reveals that E increases with q^2 and $q \propto 1/R$ because $q = j_{ln}/R$. Predominant localisation in the $Al_{0.3}Ga_{0.7}As$ layers takes place, however, due to the effective potential being smallest in the $Al_{0.3}Ga_{0.7}As$ region (refer also to Fig. 6, lower plots).

In Fig. 7, a plot of the ground-state energy versus the NWSL radius is shown for the asymmetrical structure with two GaAs material layers. As expected, the energy increases strongly with decreasing radius (refer to the above-mentioned argument). The computed results also show that the ground-state energy is above the $Al_{0.3}Ga_{0.7}As$ conduction band-edge when $R < 50$ Å. Nevertheless, these states are all bound in the z-direction.

5. Conclusions

We have analysed computationally energy levels in nanowire superlattice structures with a cylindrical cross-section by solving associated PDE eigenvalue problems. We have demonstrated that there exist qualitative differences in the electronic wavefunctions between NWSL structures consisting of: (a) $N + 1$ barrier layers and N well layers; and (b) N barrier layers and N well layers where N is an integer. In addition, we have compared eigenvalues and eigenfunctions obtained in our calculations with exact Kronig–Penney model results. Our modelling results have confirmed that finite symmetrical NWSL structures with increasing numbers of N behave like an infinite NWSL structure. However, in the case of asymmetrical finite NWSL structures, a bound state exists which finds no analogue in the symmetrical NWSL structure or in the Kronig–Penney model case corresponding to an infinite (periodic) NWSL structure. In this paper, special attention has been given to the examination of quantum-localisation effects in NWSL structures for NWSL radii above, at and below the so-called critical radius. Our numerical results have confirmed that no material localisation takes place in the NWSL structure for a radius equal to the critical radius. Furthermore, inversion of envelope-function localisation occurs at radii below the critical radius where ground-state envelope functions predominantly are located in the $Al_{0.3}Ga_{0.7}As$ material layers.

Acknowledgements

Two of the authors, LCLYV and CG, were supported by an NSF CAREER award (NSF Grant No. 9984059). LCLYV acknowledges also support of the Balslev Foundation.

References

[1] G. Bastard, Wave Mechanics Applied to Semiconductor Heterostructures, Les Editions de Physique, Les Ulis, 1988.
[2] M.T. Björk, et al., One-dimensional steeplechase for electrons realized, Nano Lett. 2 (2002) 87–89.
[3] M.G. Burt, The justification for applying effective-mass approximation to microstructures, J. Phys.: Condens. Matter 4 (1992) 6651–6690.
[4] Femlab Reference Manual, version 2.3, Comsolab, 2002.
[5] F. Gelbard, K.J. Malloy, Modeling quantum structures with BEM, J. Comput. Phys. 172 (2001) 19–39.
[6] M.S. Gudiksen, et al., Growth of nanowire superlattice structures for nanoscale photonics and electronics, Nature 415 (2002) 617–620.

[7] L.C. Lew Yan Voon, M. Willatzen, Electron states in modulated nanowires, J. Appl. Phys. 93 (12) (2003) 9997–10000.
[8] R.V.N. Melnik, M. Willatzen, Bandstructures of conical quantum dots with wetting layers, Nanotechnology 15 (2004) 1–8.
[9] R. Solanki, et al., Atomic layer deposition of ZnSe/CdSe superlattice nanowires, Appl. Phys. Lett. 81 (2002) 3864–3866.
[10] A. Quarteroni, R. Sacco, F. Saleri, Numerical Mathematics, Springer-Verlag, Berlin, 2000.
[11] J. Wang, et al., Highly polarized photoluminescence and photodetection from single indium phosphide nanowires, Science 293 (2001) 1455–1457.
[12] Y. Wu, R. Fan, P. Yang, Block-by-block growth of single-crystalline Si/SiGe superlattice nanowires, Nano Lett. 2 (2002) 83–86.